Novel optical phenomena with photonic crystals

Chiyan Luo[a], Steven G. Johnson[a], Marin Soljačić[a], J. D. Joannopouls[a], and J. B. Pendry[b]

[a]Dept. of Physics, Massachusetts Institute of Techonology, Cambridge, MA, USA 02139
[b]The Blackett Laboratory, Imperial College, London, United Kingdom SW7 2BZ

ABSTRACT

In this work we present an introduction to photonic crystals by discussing the basic concepts and principles behind these artificial materials, as well as their abilities to control light and enable unusual optical phenomena. We will focus on specific examples including (1) negative refraction of light, (2) the superprism effect (anomalous electromagnetic dispersion), and (3) the possibility of superlensing (subwavelength focusing). These are very general results based on direct solutions of Maxwell's equations, and can consequently be of relevance to many areas of science and technology.

Keywords: photonic crystals, negative refraction, superlens, superprism

1. INTRODUCTION TO PHOTONIC CRYSTALS

Photonic crystals are materials whose electromagnetic (EM) properties vary periodically on a lengthscale comparable to the wavelength of light, particularly with strong contrast. Within such materials, the propagation of classical EM waves is determined by the detailed structures of the photonic lattice, and is completely governed by Maxwell's equations. The crystal structure in three dimensions can be very complicated and thus affect light propagation in a highly nontrivial way, sometimes exhibiting spectacular features that are unfamiliar in conventional optics of a uniform material.

The physics of photonic crystals[1, 2] are often compared to those of crystalline solids, in which the periodic scattering potentials provide a similar modification to the quantum-mechanical motion of electrons. The basic problem is to determine the modes of light propagation in a given photonic lattice, usually described by a position-dependent permittivity $\epsilon(\mathbf{r})$. The Maxwell's equations can be casted in a stationary-state form as[3]

$$\mathbf{\Theta F} = \frac{\omega^2}{c^2}\mathbf{F}, \tag{1}$$

where $\mathbf{\Theta}$ is a position-dependent Hermitian operator containing $\epsilon(\mathbf{r})$, $\mathbf{F}$ is the EM field, and ω is the frequency of the eigenstate (for example, when $\mathbf{F}$ is the magnetic field $\mathbf{H}$, $\mathbf{\Theta} = \boldsymbol{\nabla} \times \epsilon^{-1}(\mathbf{r})\boldsymbol{\nabla}\times$). The form in Eq. (1) provides an explicit analogy to the Schrödinger's equation, and the square eigen-frequency ω^2/c^2 corresponds to the energy eigenvalue in quantum mechanics. The solution to Eq. 1 in a photonic crystal can be classified using the fundamental concepts in the band theory of electrons. According to the *Bloch's theorem*, the eigenmode $\mathbf{F}$ can be made *Bloch-periodic* with a *Bloch wavevector* $\mathbf{k}$ that lies within a *Brillouin zone*. The eigenfrequency ω then emerges as a function of $\mathbf{k}$ and band index n: $\omega = \omega_n(\mathbf{k})$, and maps out the *photonic band structure* as $\mathbf{k}$ is varied throughout the Brillouin zone. A *photonic band gap* may result for a frequency range in which no eigenmodes are allowed. Actual photonic band structures may be calculated using the numerical techniques developed in the studies of electron band structure, such as plane-wave expansion[4] or the Korringa-Kohn-Rostoker method.[5] On the other hand, there exist a number of physical differences between EM eigenmodes in photonic crystals and electron Bloch waves in crystals. Of particular importance is the extreme wide generality of the principle of photonic crystals. This is because there are no fundamental lengthscales in Maxwell's equations, and the band structure may be scaled to arbitrary frequencies provided the photonic lattice is correspondingly scaled. A system designed at the microwave regime can therefore be "scaled" to other wavelengths, e.g. the optical regime, using identical dimensionless parameters. This is vastly different from the electronic case in which the

Send correspondence to C.L.: E-mail: chiyan@mit.edu, Telephone: 1 617 253 5482, Fax: 1 617 253 2562, Address: Room 12-111, Massachusetts Institute of Techonology, 77 Massachusetts Avenue, Cambridge, MA 02139

UV/Optical/IR Space Telescopes: Innovative Technologies and Concepts, edited by Howard A. MacEwen, Proceedings of SPIE Vol. 5166 (SPIE, Bellingham, WA, 2004) · 0277-786X/04/$15 · doi: 10.1117/12.507491

Bohr radius sets a natural lengthscale for the system. Moreover, as the EM waves are vector fields, the photonic band structure contains information about light polarization and is richer than its scalar-wave counterpart in the electronic problems. Finally, it is worth noting that numerical results of photonic band structure are essentially *exact* within the linear response approximation and can be more reliable than those of electronic band structures, which are almost always complicated by the effects of electron-electron interaction and Fermi statistics.

Photonic crystals have been proposed to revolutionize the generation[6–10] and propagation[11–16] of light waves. Indeed, the existence of a photonic band gap in a range of frequencies prohibits light propagation in all possible directions. This has led not only to novel photon-atom bound states that alter the fundamental physics of light emission, but also to the concept of basic building blocks for optical materials that can used to construct practical devices for applications. Deliberate defect structures inside the band gap adds a new design dimension for versatile light control. Ultrahigh-Q cavities may be introduced as point defects in a perfect crystal to realize resonance channel add-drop filters and ultra-low threshold lasers. Channels for efficient light transportation are formed by line defects which can guide light through very sharp corners. Furthermore, by combining the index-guiding mechanism of slab waveguides with two-dimensional photonic band gap effects, control and manipulation of light in full three dimensions can be realized with present planar lithographic techniques. These developments echo with the past band-gap engineering in semiconductor electronics and suggest that photonic crystals may be used to tailor the properties of light in much the same way.

This paper is about photonic crystals as a new class of bulk optical materials. The pioneering works on this subject are those of Lin et al,[17] Kosaka et al,[18] Gralak et al,[19] and Notomi.[20] Via experimental and computational means, these authors explored the effects of photonic-crystal dispersion relations on the direction of light flow and discovered the superprism phenomenon as well as an effective *negative* index of refraction for light. Recently, negative refractive index has been observed in microwave left-handed materials[21–23] and was further proposed to lead to the formation of a *perfect* lens.[24] The superprism effect has also been studied in detail in two-dimensional (2D) triangular optical lattices[25–28] and in three-dimensional (3D) photonic crystals.[29,30] In this paper, we discuss using photonic crystals to achieve negative refraction of light *without using a negative index*.[31–34] We then distinguish two superprism effects and discuss their different influence on radiation propagation. In addition, we extend our analysis to evanescent waves, and demonstrate the possibility of focusing light to subwavelength resolutions using photonic crystals. All of these novel optical phenomena are a direct consequence of Maxwell's equations and thus should have extremely wide validity, making photonic crystals an attractive material candidate for designing novel technologies in many disciplines of science and technology.

2. NEGATIVE REFRACTION WITHOUT A NEGATIVE INDEX

Let us first consider light refraction from vacuum into an isotropic uniform material, using a coordinate system in which the interface plane is perpendicular to the z axis. Because the system is invariant under an arbitrary translation in the interface plane, the refraction process will conserve the wavevector components parallel to the interface. From the dispersion contours (diagrams of wavevector $\mathbf{k}$ for propagation at a constant frequency ω) for both mediums, one can find the wavevector of the refraction modes corresponding to the incident ω and surface-parallel wavevector. The direction of refraction may then be determined by finding the direction of the Poynting's vector for the refraction modes that propagates away from the interface. This procedure is illustrated in Fig. 1 for a material with permittivity ϵ and permeability μ. In the plane of refraction, the dispersion contours of both vacuum and the material are circles given by $\mathbf{k}^2 = \epsilon\mu\omega^2/c^2$. For $\epsilon > 0$ and $\mu > 0$, the direction of the Poynting vector is along that of the wavevector, and thus the refraction angle satisfies the usual Snell's law $\sin\theta_{inc} = \sqrt{\epsilon\mu}\sin\theta_{refr}$, where θ_{inc} and θ_{refr} are incidence and refraction angles as marked in Fig. However, if $\epsilon < 0$ and $\mu < 0$ as in a left-handed material,[21,22] the EM modes are the so-called *backward waves* and their Poynting vector must be anti-parallel to the wavevector, a property also known as having a *negative group velocity*. In order for the refracted wave to propagate away from the interface, the mode with the negative k_z becomes the refraction mode, which travels on the *negative* side of the surface normal. This gives rise to a Snell's law,

$$\sin\theta_{inc} = -\sqrt{|\epsilon\mu|}\sin\theta_{refr}, \tag{2}$$

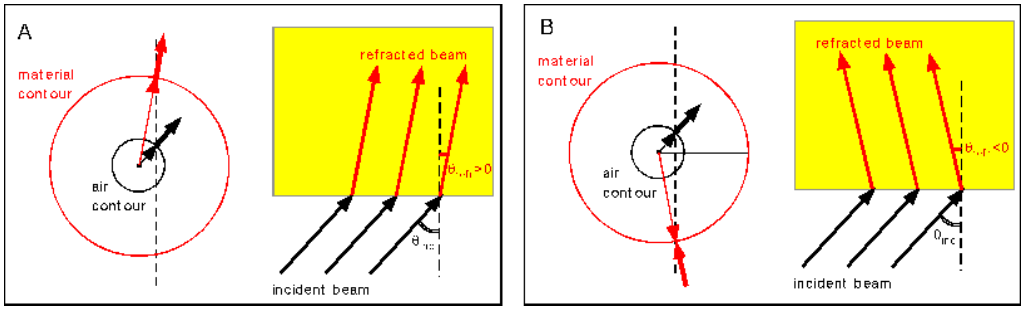

Figure 1. (Color) Illustration of refraction in uniform media. A: positive refraction in a medium with $\epsilon > 0$ and $\mu > 0$. B: negative refraction in a medium with $\epsilon < 0$ and $\mu < 0$. In each subfigure, the left panel is the wavevector diagram, and the right panel shows the propagation directions for the incident and refraction beams. Thick arrows indicate group-velocity directions, and thin arrows stand for phase-velocity directions.

with a *negative* index of refraction. This possibility of a negative refracted index has been confirmed experimentally[23] and become one of the many experimental proofs for the existence of metamaterials with *epsilon* < 0 and $\mu < 0$.

The situation becomes more interesting if the second material is a photonic crystal. The interface now has a lowered translational symmetry along only discrete surface lattice constants, leading to the conservation of the surface-parallel Bloch-wavevector within the surface Brillouin zone. To find the refraction mode in the photonic crystal, one needs to calculate the dispersion contour at an arbitrary frequency ω for the photonic crystal. It can be shown[35] that the gradient vector $\partial\omega/\partial\mathbf{k}$ to such a dispersion contour continues to give the group velocity, i.e. the spatially-averaged Poynting vector, of the photonic modes. The above approach can thus be generalized to the case with photonic crystals. Due to the strong optical modulation in the crystal, the shape of the dispersion contour may differ considerably from being circular, providing a variety of interesting refraction possibilities.

As a specific example, we consider a 2D square lattice of air holes in dielectric $\epsilon = 12.0$ with lattice constant a and hole radius $r = 0.35a$. We consider light waves propagating in the plane of 2D periodicity and having a magnetic field parallel to the cylinders (TE modes). The photonic band structure of this crystal can be numerically calculated using planewave expansion,[36] and is shown as the dispersion contours in Fig. 2. Here we observe that due to the negative-definite effective mass tensor $\partial^2\omega/\partial k_i \partial k_j$ at the M point, the frequency contours are *convex* in the vicinity of M and have inward-pointing group velocities. According to our approach, for frequencies that correspond to all-convex contours near M, negative refraction occurs as illustrated in Fig. 2. The distinct refracted propagating modes are determined by the conservation of the frequency and the wavevector component parallel to the air/photonic-crystal surface. If the surface normal is along ΓM [(11) direction], and the contour is everywhere convex, then an incoming planwave from air will couple to a single Bloch mode that propagates into this crystal on the *negative* side of the surface normal. We have thus realized negative refraction in the first band.

To verify negative refraction, we proceed with a computational experiment using Finite-Difference Time-Domain (FDTD) simulations. Here, a continuous-wave (CW) Gaussian beam of frequency $\omega_0 = 0.195(2\pi c/a)$ and a half width $\sigma = 1.7(2\pi c/\omega_0$ is launched at 45° incidence toward the (11) crystal surface of our photonic crystal and subsequently refracts into it. A snapshot of this refraction process is shown in Fig, which shows that the overall electromagnetic energy indeed travels on the reversed side of the surface normal. If we look closely at the refracted field profile in the photonic crystal, we can see that there are constant-phase regions lying on parallel straight lines and forming "phase-fronts" in the photonic crystal. However, there are multiple ways of constructing parallel lines connecting these discrete regions, corresponding to multiple choices of phase-front definitions. This fact reflects that, in a photonic crystal, $\mathbf{k}$ is only defined up to a reciprocal lattice vector $\mathbf{G}$. For the present situation, we choose the phase fronts for the refracted beam to be the set of constant-phase lines with the largest wavelength in the crystal, which corresponds to the smallest $|\mathbf{k}|$ and hence the unique $\mathbf{k}$ representing the Bloch-phase in the first Brillouin zone. The normals of the phase-fronts defined in this way now

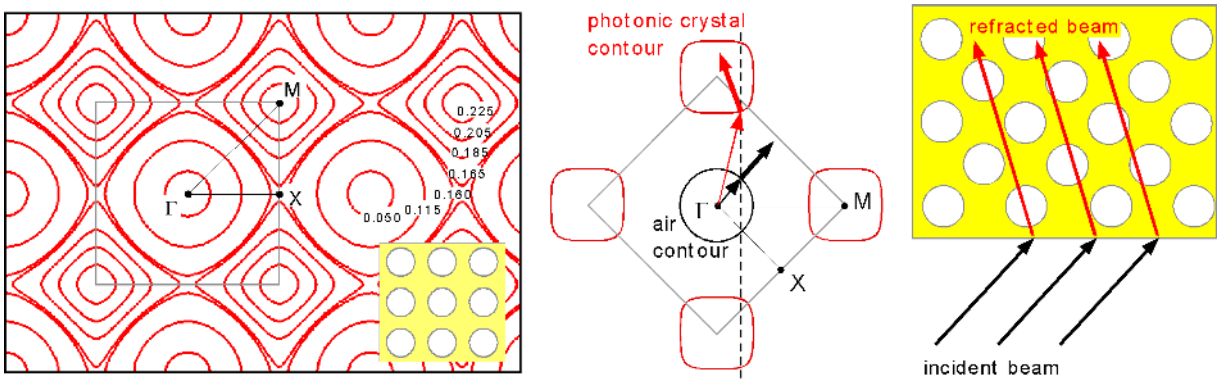

Figure 2. (Color) Left panel: dispersion contours of the first band of a model photonic crystal, drawn in the repeated zone scheme. Frequency values are in units of $2\pi c/a$. Middle panel: wavevector diagram of negative refraction in this photonic crystal. Thick arrows indicate group-velocity directions, and thin arrows stand for phase-velocity directions. Right panel: diagram of refracted rays in the actual crystal.

points toward the *positive* side of the surface normal, i.e. the phase velocity exhibits *positive* refraction.

It is clear from this example that the notion of a backward wave or a left-handed material is in fact not a prerequisite for negative refraction. The physics of our example differs from those of left-handed materials in that the lowest band now has $\mathbf{k} \cdot \partial\omega/\partial\mathbf{k} \geq 0$ everywhere within the first Brillouin zone, meaning that the group velocity is never opposite to the Bloch-wavevector $\mathbf{k}$. In this sense, we are operating in a regime of forward waves and positive effective index. Such a scenario can also happen in a right-handed medium with hyberbolic dispersion relations induced by anisotropy. For example, the TE modes in a uniform nonmagnetic medium with dielectric tensor:

$$\tilde{\epsilon} = \begin{pmatrix} \epsilon_1 & 0 \\ 0 & \epsilon_2 \end{pmatrix}, \tag{3}$$

with $\epsilon_1 > 0$ and $\epsilon_2 < 0$, have a dispersion relation $k_2^2/\epsilon_1 - k_1^2/|\epsilon_2| = \omega^2/c^2$. Similar negative refraction will then happen on the (01) surface. Again, the phase velocity always makes an acute angle with the group velocity.

It should be noted, however, that the analogy of photonic crystals with high dielectric contrast to a uniform medium is usually accurate only when the frequency is in the lowest few bands *and* away from the band edge. As the frequency approaches the band edge or goes into higher photonic bands, each photonic mode begins to exhibit strong, wavelength-scale spatial modulations, and more than one distinct modes will occur for the same frequency. Absent from an effective medium theory but important for the optical properties of the crystal, these additional features present difficulties in general in regarding photonic crystals in their higher bands as effective *uniform* materials.

As an example, let us look at an example in a 3D photonic crystal. We consider a body-centered cubic lattice of cube-shaped air voids in dielectric $\epsilon = 18$, whose band structure is shown in Fig. 4. The side of the conventional bcc cell is a, and the side of the void cubes is taken to be $0.75a$. Marked out in the shaded region in the third band is a large frequency range within which the dispersion surface of the photonic crystal forms a single all-convex, near-spherical surface and is larger than that of air. This guarantees that the crystal in this frequency range exhibit negative refraction for all incident angles (AANR) and precludes the possibility of near band-edge operation. Because the third band exhibits negative group velocity ($\mathbf{k} \cdot \partial\omega/\partial\mathbf{k}$) the 3D crystal may be regarded as having an effective index n_{eff} less than -1. However, since there is only one band in this frequency range in full 3D, the refraction phenomena will be strongly polarization dependent. For example, along the (001) direction, the two degenerate polarizations of normal-incidence radiation in vaccum and the single-degenerate photonic-crystal mode belong to different irreducible representations of the surface symmetry group. As a result, they do not couple with each other, and thus the (001) surface should *not* be used as the interface with air. To fix this problem, the (101) surface, whose symmetry group has different irreducible representations for the two

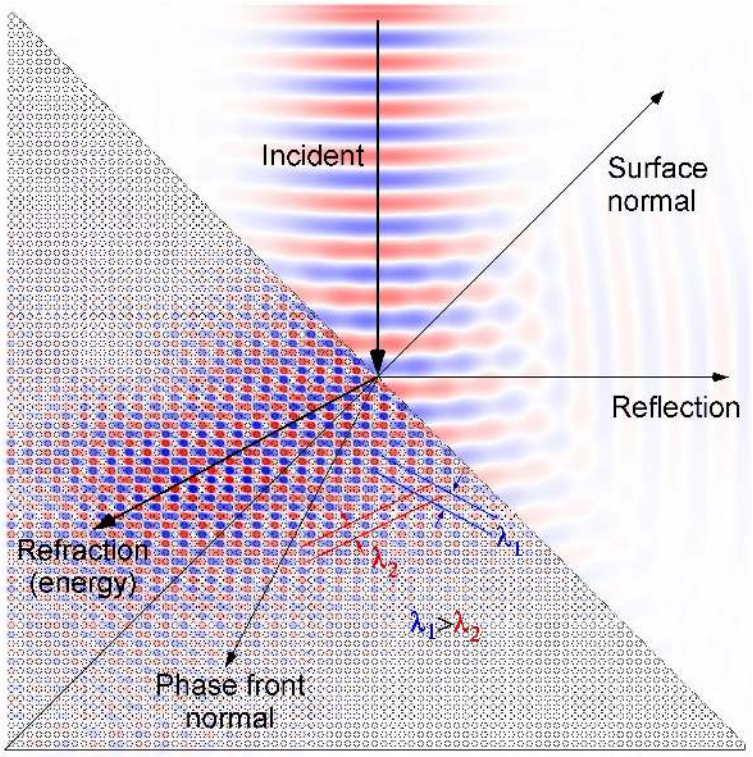

Figure 3. (Color) FDTD simulation of negative refraction in a photonic crystal. Shown is the pattern for the magnetic field **H** perpendicular to the plane (red for positive and blue for negative values). The dielectric boundaries are outlined. The arrows and texts illustrate the various important directions for this effect. Also shown in red and blue lines are two possible ways of construction phase fronts from the field pattern. We choose the set of phase front with the maximum wavelength (λ_1) to be that of the refracted beam.

polarizations, should be used. Along the normal direction on this surface, the crystal mode favors coupling with waves polarized along $(10\bar{1})$ and does not couple with those polarized along (010). This dependence of coupling efficiency on surface termination and polarization direction illustrate the important difference between photonic crystal in their higher bands and an *isotropic*, *uniform* medium and a negative refractive index.

It should become clear from this discussion that negative refraction is an unambigous effect made possible by 2D and 3D photonic crystals. In passing we note that in the above we have mainly relied on the method of dispersion surfaces in our understanding. This method is powerful in finding the direction of the refracted waves for an incident planewave, but does not yield information concerning the detailed coupling efficiency for such processes. This deficiency, however, is not a great difficulty for two reasons. On the one hand, Fig. 3 shows that the coupling efficency itself can be very large in the frequency regions we are looking at. On the other hand, given the material into which light waves are refracted from vacuum, the direction of refraction is universal, while the intensity of the refracted wave depends greatly on the details of the material and holds a less general significance. We thus postpone a detailed discussion on the issue of coupling to Section 3.

3. THE SUPERPRISM EFFECT

In this section, we discuss two types of effects that exhibit anomalously large electromagnetic dispersion, whose magnitude can be orders of magnitude larger than the intrinsic dispersion of dielectric materials. The first type was introduced by Kosaka et al,[18] and makes main use of group-velocity dispersion properties of photonic crystals. The other type was due to pioneering work of Lin et al[17] and depends primarily on a photonic crystal's phase-velocity dispersion. As we will see, these are two physically different but closely related effects

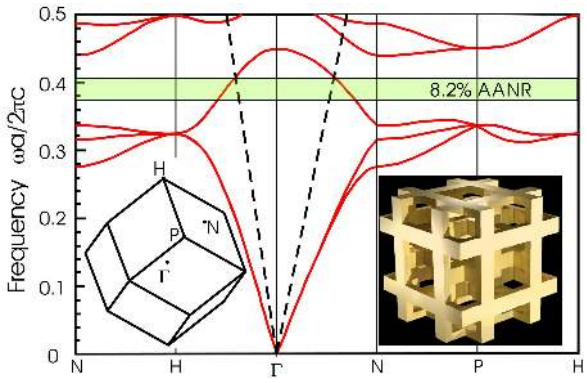

Figure 4. (Color) Band structure (red) of a bcc lattice of air cubes in dielectric whose parameters are given in the text. In the shaded AANR frequency range (green) the photonic crystal exhibits negative refraction for incoming radiation for all angles. The dashed lines are light lines along ΓH and ΓN. Insets are the shape and special symmetry vertices of the first Brillouin zone and a computer rendering of the actual crystal.

that correspond to two extreme regions of the photonic-crystal dispersion surface. Hence, we will use the term *superprism effect* to refer to either one of them.

Let us continue using our model photonic crystal of Section 2 as an example, and continue to consider refraction on the (11) surface. In the superprism effect of the group velocity type, a small change in the parameters of the incident planewave (incident angle θ_{inc} or frequency ω) gives a large change in the refraction angle θ_{refr} of the Bloch wave in the crystal. Here, for example, we take the parameter to be θ_{inc} at a constant ω and consider the change $\Delta\theta_{refr}$ in the refraction direction by a change $\Delta\theta_{inc}$ in the incident direction, seeking the condition for large $\Delta\theta_{refr}/\Delta\theta_{inc}$. As in Section 2, θ_{refr} is the gradient direction of the dispersion surface, and $\Delta\theta_{refr}$ stands for the difference in the gradient directions of two nearby refraction modes on the dispersion surface. On the other hand, $\Delta\theta_{inc}$ corresponds to a change in the transverse wavevector and measures the distance in **k**-space of the two nearby refraction modes up to an angular factor. Thus, the condition for large $\Delta\theta_{refr}/\Delta\theta_{inc}$ can be regarded to be the condition for *large curvature* locations, i.e. *sharp corners*, on the dispersion surface. For example, near the photonic band edge, the radius of the dispersion contour $r_{\mathbf{k}}$ becomes small and exhibits large curvature, giving a large angular amplification

$$|\Delta\theta_{refr}/\Delta\theta_{inc}| \approx \frac{\omega}{cr_{\mathbf{k}}} \tag{4}$$

(see Fig. 5). Note that as $r_{\mathbf{k}} \to 0$ the angular amplification is unlimited, indicating that arbitrarily strong dispersion is in principle possible. Moreover, similar behaviors can also occur for small changes in the frequency of light, and can be expected near other sharp corners such as X-point as well. Furthermore, this group-velocity-based superprism effect does not require a complete photonic band gap in general and may persist even for systems with a small dielectric contrast (in which case, of course, there are usualy more than one refraction beams and not all of them experience this superprism effect at the same time).

In the superprism effect above, the agile beam steering occurs only for light waves travelling inside the crystal. For beams entering a prism-shape photonic crystal, their large angular separation disappears once the light exits the photonic lattice from an output facet. This is because the Bloch-wavevector **k**, or the phase velocity of light in the crystal, is the key quantity responsible in determining the final beam direction: the component of **k** along the exit surface must be conserved. Since the group-velocity superprism effect occurs in a region of the dispersion surface with a large curvature, despite the large change in the direction of $\partial\omega/\partial\mathbf{k}$, the change in **k** inside the crystal is actually very small. As a result, a large crystal is needed to spatially separate light beams using the group-velocity basied superprism effect as shown in Fig. 5. It is natural to wonder whether a superprism effect in **k** itself would be possible, in which the direction of light outside the crystal can be steered with high sensitivity. The large space region used to separate light may then be replaced by air and the size of the crystal itself may

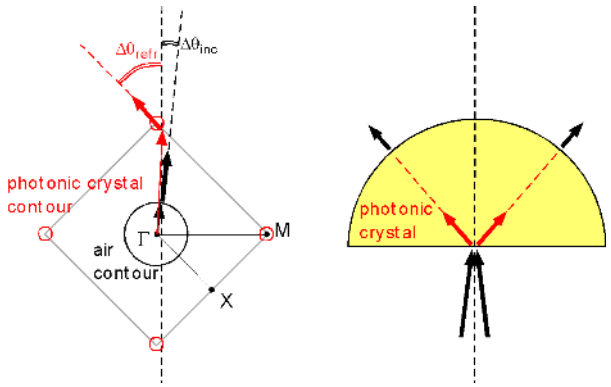

Figure 5. (Color) Left panel: dispersion-surface analysis of group-velocity based superprism effect in our model photonic crystal, using the same notation as in Fig. 2. Right panel: illustration of a possible way of realizing this superprism effect in a semi-circular shaped photonic crystal (yellow). The thick red arrows indicate the group-velocity directions inside the photonic crystal.

then be reduced. According to the experiments by Lin et al,[17] a dispersion increase of roughly 20% can be expected for frequencies approaching the photonic band gaps. This magnitude of dispersion in **k**, however, is comparable to that in a classical grating operating in the grazing-angle limit and about an order of magnitude smaller than that predicted by Eq. 4. We show below that photonic crystals can actually be used to achieve a much larger magnitude of phase-velocity dispersion.

A large change in the Bloch wavevector **k** corresponds to a large change in the component of **k** that is parallel or perpendicular to the interface. Since the change in the parallel **k**-component is the same as that in the incident radiation, Δk_{inc}, which is small for a small change in incident angle θ_{inc} or frequency ω, we need to change the perpendicular component, which we call Δk_{refr}. That $\Delta k_{refr}/\Delta k_{inc}$ is large for a small but continuous range of Δk_{inc} means that the corresponding part of the dispersion surface is almost perpendicular to the interface and *flat*. This criterion points to a regime of dispersion surface different from what we studied above–a region with very small curvature. In the dispersion contours of Ref. 2, such flat regions do exist for frequencies between the X band-edge and the M band edge. In fact, in this frequency region an extremely flat part occurs between concave and all-convex contour shapes, with a radius of curvature much larger than that of a uniform medium with a dielectric constant as high as $\epsilon = 12$. To realize the superprism effect with this part of dispersion surface, an arrangement such as that shown in Fig. 6 can be employed. Here an extra prism of a high-index material $\epsilon = 12$ is added before the incidence (11) facet of the photonic crystal so that the flat portion of the dispersion surface is perpendicular to the interface and can be coupled to. In this way, a tiny change in the incident angle can be reflected in a huge change in the refracted wavevector, steering a beam exiting the device within a large range of outgoing directions. Similar analysis can also be applied to frequency dispersions, and a tiny change in the incoming frequency can also modify the Bloch wavevector **k** greatly. Moreover, we note that in the present effect the occurrence of flat dispersion surfaces requires strong dielectric constant, which is similar to negative refraction in photonic crystals. It is, however, different from the superprism effect based on group velocities in which sharp dispersion-surface corners appear even for small index contrast or small filling ratios. Furthermore, it should be noted that this effect is also similar to situations in elementary refraction or diffraction gratings when one of the output beams occurs at grazing angles. In those latter cases $\Delta k_{refr}/\Delta k_{inc}$ can approach large values as well for a very small range of Δk_{inc} in which k_{refr} approaches the grazing condition. The key difference in our photonic crystal is that the dispersion surface can be much flatter, permitting a much larger Δk_{refr} for a given Δk_{inc}.

Finally we study the energy transmission properties in the superprism phenomena. For simplicity, here we mainly focus on the effect due to the group velocity, and entirely similar conclusions may be extended to the effect with phase velocities as well. We consider a wave going through a finite slab of photonic crystal and study the properties of the transmission using the well-established scattering-matrix approach.[37] If the incident wave is

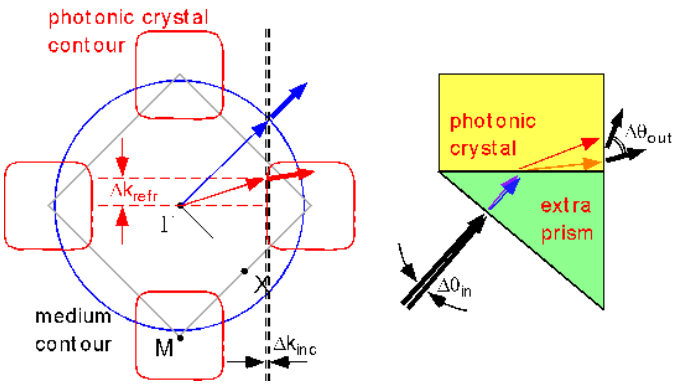

Figure 6. (Color) Left panel: dispersion-surface analysis of phase-velocity based superprism effect in our model photonic crystal, using the same notation as in Fig. 2. Right panel: illustration of a possible way of realizing this superprism effect in a prism-shaped photonic crystal (yellow), with an extra prism (green) added before the incidence interface. The thin arrows indicate the Bloch-wavevector directions inside the prisms.

also a finite-sized beam, a lateral shift $\mathbf{L}$ will occur due to the refraction at the crystal interfaces. The magnitude of $\mathbf{L}$ may thus be used to measure the angular dispersion inside the crystal.* We represent a finit-sized beam by a superpositions of planewaves of different transverse wavevector $\mathbf{k}_p$'s whose weights peak at a certain $\mathbf{k}_p$. For very wide beams, $\mathbf{L}$ can be estimated by the following equation,

$$\mathbf{L} \approx -\frac{\partial Arg[t(\mathbf{k}_p), \omega]}{\partial \mathbf{k}_p}, \tag{5}$$

where $t(\mathbf{k}_p, \omega)$ is the complex transmission coefficient as a function of $\mathbf{k}_p$ and ω. In this approach, both the transmission efficiency $|t|^2$ and the lateral shift $\mathbf{L}$ can be obtained to construct a complete picture of the refraction process.

For analytical convenience, we now consider a slab of 2D "checkerboard" crystal, which is a square lattice of (11)-oriented, alternating square regions of dielectric $\epsilon = 12$ and vacuum. The slab is taken to be symmetric and has a thickness of 25.5 periods (1 period along the thickesness direction is $\sqrt{2}a$ where a is the lattice constant of the square lattice). The calculated transmission $|t|^2$ and lateral shift L for incident radiation having a common transverse wavevector $k_x = 0.1(2\pi/\sqrt{2}a)$ for frequencies around the first band edge are shown in Fig. 7. As frequency increases toward the band edge, the envelope trend of the lateral shift L moves from positive to negative, confirming the negative refraction discussed in the previous section. Moreover, this envelope of L becomes more and more negative as the band edge is approached and eventually diverges $L \to -\infty$ at the edge, depicting the super-dispersive nature near the photonic band edge. However, both $|t|^2$ and L exhibits oscillatory behaviors. These oscillations result from interference effects between interfaces, and larger osccilation amplitudes correspond to weaker coupling strength between the photonic modes and the external planewave. Since the oscillations in $|t|^2$ and L grow stronger and stronger as the band edge is approached, the intensity of the refracted wave inside the crystal generally becomes weaker and weaker and decays continuously to zero in this limit. In the superprism effect, the huge dispersion induced by photonic crystals always occurs near a photonic band edge, and thus such an effect always comes with a sacrifice in coupling efficiency, which can be a rather serious problem for the superprism effect to be useful in potential applications.

A practical remedy to this problem is to design some appropriate photonic-crystal structures to improve the rate at which the coupling efficiency drops near the band edge, so that a relatively strong transmission can be maintained in a region of simultaneously high dispersion. This brings up the issue of engineering crystal interfaces for better transmission, a possibility recently discussed by Baba in the context of a particular type of interface.[38]

*It should be noted that $\mathbf{L}$ contains information about both the refraction angle and the wave interference between the crystal interfaces and is a quantity beyond geometric optics.

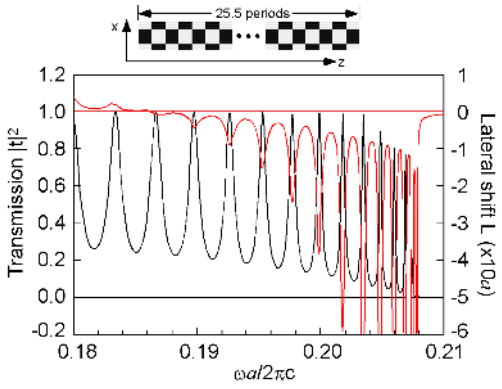

Figure 7. (Color) Calculated transmission $|t|^2$ (black) and lateral shift L (red) for a photonic-crystal slab. The incident radiation is assumed to have a trasverse wavevector $k_x = 0.1(2\pi/\sqrt{2}a)$. The inset shows the shape of the structure (only one period along the transverse direction x is shown).

Here we demonstrate that a systematic method for improving the coupling efficiency into bulk crystals is to use adiabatic-tapering interfaces similar to that in the waveguide field.[39] The design criteria for the taper is simply that it should provide a continuously and slowly varying environment for light to go from one medium into the other, in the course of which no photonic band gap should appear. For tapering the checkerboard crystal to free space, we can simply use intermediate cells with the same lattice constant a but reduced-size dielectric rods, gradually bringing the rods to zero size. Fig. 8 shows the calculated transmission and lateral shift results for the same photonic crystal in Fig. 7 with extra taper layers on each side to provide a smooth transition from the photonic crystal to vacuum. As can be seen clearly, the additional taper layers greatly help reduce the Fabry-Perot oscillations and increases the transimssion to near unity for a wide range of frequencies even for a mere taper thickness of 4 periods. This improvement becomes better with an increasing number of tapering layers, and for a 8-period taper, for example, lateral shifts of more than $100a$, corresponding to an approximate refraction-angle magnitude larger than 80°, are realizable with an efficiency higher than about 80%. Note that the position where L crosses 0 will be slightly modified in the presence of the taper structure by the lateral shifts of the transition layers, which are usually positive. In general, as in the theory of waveguides,[39] the envelope of the reflection coefficient is inversely proportional to the square of the taper length for linear tapers. Therefore, with sufficiently long tapers, good coupling can always be achieved very close to the band edge, solving the efficiency problem in the extraordinary dispersion processes of photonic crystals.

4. SUBWAVELENGTH IMAGING

In the previous sections we have seen that photonic crystals can be used to create unusual phenomena by controlling the properties of propagating waves. In this section, we examine the effect of photonic crystals on evanescent waves, which are characterized by $|\mathbf{k}|_p > \omega/c$. These waves represent the very fine, subwavelength details that decay rapidly away from the source. Although conventional optical instruments such as lenses and mirrors can focus propagating waves, they are powerless in transforming evanescent waves, which remains exponentially small after transmission. One novel way to manipulate evanescent waves was to use a slab of left-handed material with $\epsilon = -1$ and $\mu = -1$, which is predicated to amplify evanescent waves.[24] Both the propagating waves and the evanescent waves emitted by a point source placed in front of the slab can then be captured by the slab and refocused into a *perfect* point image behind the slab. Here we show that a slab of negative-refractive photonic crystals discussed in Sec. 2 can be used to amplify a range of evanescent waves and to create focused images with subwavelength details.

We now focus on a 2D photonic crystal with a shape shown in Fig. 9A, a configuration very similar to the crystal studied in Sec. 2 and more efficient for numerical calculation of transmission. For this crystal, a frequency range exits where the negative refraction effect described in Sec. 2 happens for propagating waves at all incident angles. Such an all-angle-negative-refraction (AANR) effect can be used to collect all the propagating waves

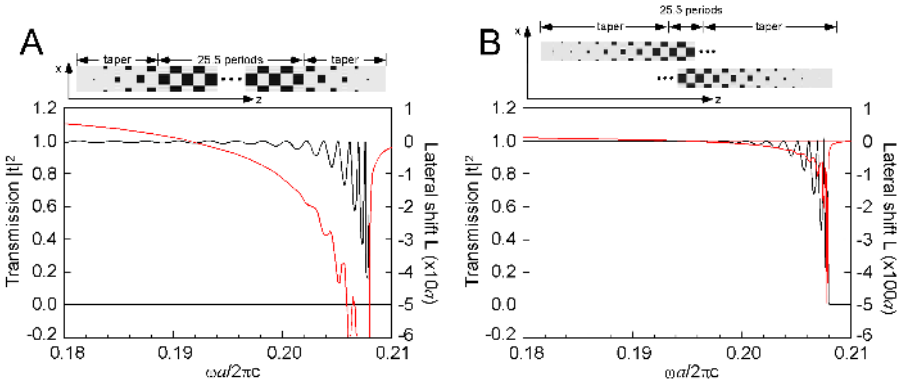

Figure 8. (Color) Calculated transmission $|t|^2$ (black) and lateral shift L (red) for a photonic-crystal slab with a taper-transition interface. The incident radiation is assumed to have a trasverse wavevector $k_x = 0.1(2\pi/\sqrt{2}a)$. The inset shows the shape of the structure (only one period along the transverse direction x is shown). A: results for a taper transition of 4 periods. B: results for a 8-period taper.

from a point source placed in front of a slab and refocus them behind it, a starting point for subwavelength imaging. Fig. 9B shows this AANR range, as well as the bound-photon band structure of a slab of the present photonic crystal. Below the light cone and inside the region of the projected band structure of the infinite crystal, the bound photon states are guided by the bulk slab; the modes inside the partial photonic band gap are the surface states guided by the air/slab interfaces. The surface modes have two bands with even and odd mirror symmetry, and their splitting become small deep in the gap where the confinement is strong. All the bound photon states are the poles of transmission for evanescent waves, and consequently they can be used to amplify incident near-fields. The crystal thickness h and its associated surface termination position are chosen so that the surface bands are very flat near the frequency $\omega = 0.192(2\pi c/a)$. In this way, evanescent waves within a range of wavevectors near $\omega = 0.192(2\pi c/a)$ can all be amplified, and images formed by AANR can be further focused to subwavelength resolutions.

We calculate the image of a TE point source behind the slab by integrating the transmission complex field for planewaves of different transverse wavevectors, using a coordinate system with x parallel to the slab and z perpendicular to the slab. The region $z > 0$ corresponds to the image region. For slightly different frequencies across the flat surface bands, the image exhibits several distinctive types of patterns, which are strongly influenced by the coupling to the surface photon states. The detailed results illustrating the delicate interplay between propagating and evanescent waves are shown in Fig. 10. For $\omega = 0.193(2\pi c/a)$, an isolated intensity maximum with width about 0.7λ can be realized in the image space, if the evanescent waves are amplified to a strength comparable to those of propagating waves. Moreover, because of the resonant nature of the present situation (no loss is assumed) and the extremely small group velocities of the bound photon modes, some transmitted evanescent waves can also have such an extraordinaryily enhanced amplitude that they dominate over other evanescent and all propagating modes. This leads to the enhanced surface resonance effect at $\omega = 0.192(2\pi c/a)$, for which large field oscillations exist near the crystal surface, and the transverse image profile becomes delocalized and no longer produce an isolated peak. Furthermore, a particularly interesting situation occurs at $\omega = 0.191(2\pi c/a)$, where the evanescent waves are amplified to such a degree that an intermediate imaging behavior results. In this case a distinct intensity peak can appear within the plane of AANR focusing with a size 0.45λ that is significantly below the wavelength, with no intensity maximum in $z > 0$. This is thus a pattern quite similar to that considered in the original perfect lens proposal. These different regimes of imaging patterns are a result of the delicate balance between far fields and near fields and are impossible to realize in conventional geometric optics. With their great flexibility and tunability, photonic crystals are thus a powerful and beautiful candidate in manipulating and focusing light on subwavelength scales, especially in the optical regime.

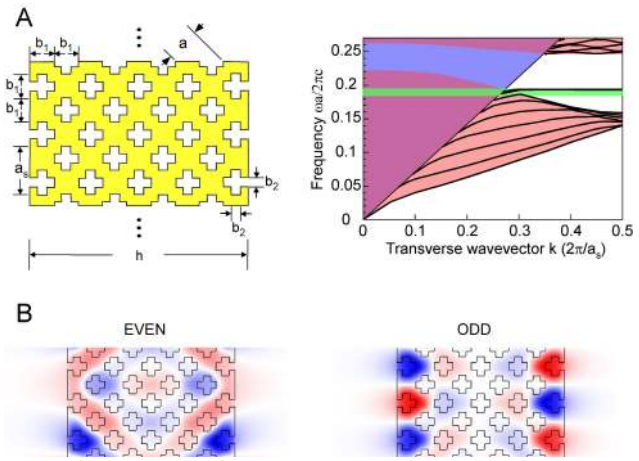

Figure 9. (Color) Bound photon modes with TE (magnetic field perpendicular to the plane) polarization in a 2D photonic crystal slab. A: Left panel: the actual photonic crystal used in calculation. The parameters are $a_s = \sqrt{2}a$, $b_1 = 0.5a_s$, $b_2 = 0.2a_s$ and $h = 4.516a_s$. Right panel: the calculated band structure of bound photon modes (black curves), plotted on top of the photonic band structure projected along the surface direction (the red filled region). The blue filled region indicates the light cone. The green range is the frequency range for AANR in this photonic crystal. B: Distribution of the magnetic field perpendicular to the plane for the surface photonic modes at $k = 0.45$ $(2\pi/a_s)$. Left and right panels represent odd and even symmetries with respect to the mirror plane at the center of the structure. Red and blue indicate positive and negative values of the magnetic field.

5. CONCLUSIONS

In this paper, we have discussed several types of novel optical phenomena enabled by photonic crystals. In the case of negative refraction, photonic crystals demonstrate a realistic example that negative refraction may occur in materials without an effective negative index. Their complex Bragg scattering effect represents anomalous electromagnetic dispersion in certain occasions, which can be further employed to manipulate the group velocity or the phase velocity of light. In properly designed crystals these processes can occur at a high efficiency. Furthermore, photonic crystals can be used to amplify evanescent waves and focus light to subwavelength resolutions. Although our discussion mainly focuses on dielectric crystals, entirely similar analysis may be applied to crystals containing metallic components, and thus these effects can be easily observed in the microwave regime. Given the extreme versatle nature of photonic crystals, we are sure that these unusual effects are only a very small part of the rich and unconventional electrodynamics made possible by photonic crystals. We hope that this paper serves as a useful guide for the reader to understand the fundamentals of photonic crystals and to discover novel applications of these new materials on their own.

ACKNOWLEDGMENTS

This work is supported in part by the NSF's NRSEC program under Award No. DMR-9400334 and the DoD/ONR MURI Grant No. N00014-01-1-0803.

REFERENCES

1. E. Yablonovitch, "Inhibited spontaneous emissionin solid-state physics and electronics," *Phys. Rev. Lett.* **58**, pp. 2059–2062, 1987.
2. S. John, "Strong localization of photons in certain disordered dielectric superlattices," *Phys. Rev. Lett.* **58**, pp. 2486–2489, 1987.
3. J. D. Joannopoulos, R. D. Meade, and J. N. Winn, *Photonic Crystals: Molding the Flow of Light*, Princeton University Press, Princeton, NJ, 1995.

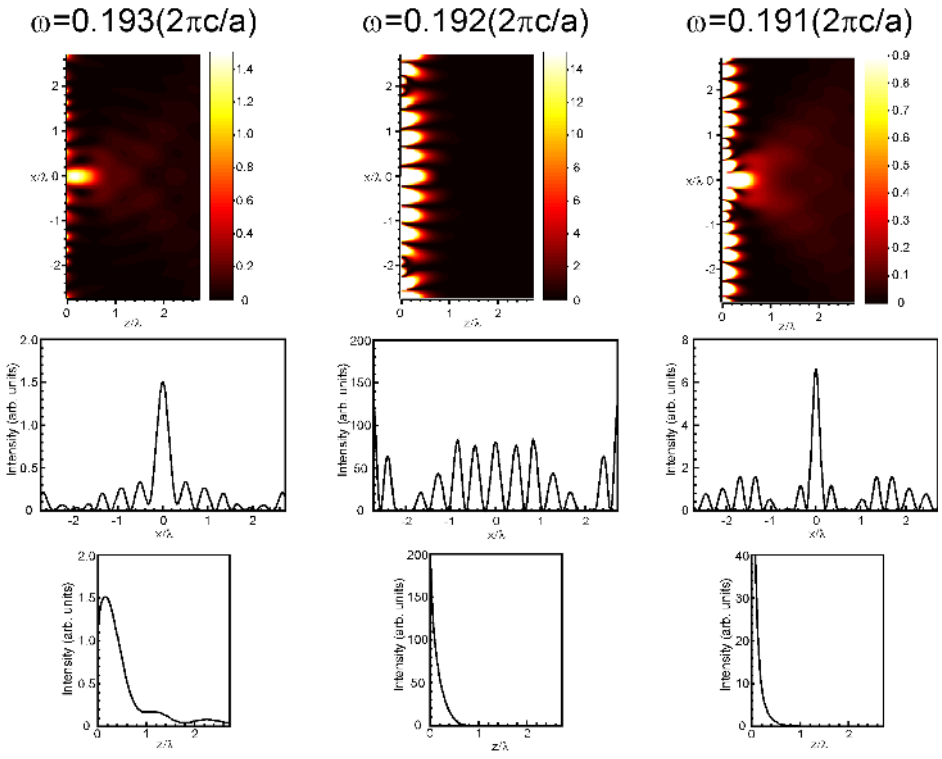

Figure 10. (Color) Calculated image intensity distribution for a photonic crystal slab in Fig. 9 illumiated with a point source. Each column corresponds to results of a different frequency. The first row is a 2D color-rendering of the image pattern. The second row plots the intensity vs the transverse coordinate x in the planes of the AANR image. The third row shows the intensity as a function of the longitudenal coordinate z at $x = 0$.

4. K. M. Ho, C. T. Chan, and C. M. Soukoulis, "Existence of a photonic gap in periodic dielectric structures," *Phys. Rev. Lett.* **65**, pp. 3152–3155, 1990.
5. K. Ohtaka, T. Ueta, and K. Amemiya, "Calculation of photonic bands using vector cylindrical waves and reflectivity of light for an array of dielectric rods," *Phys. Rev. B* **57**, pp. 2550–2568, 1998.
6. S. John, "Quantum electrodynamics near a photonic band gap: photon bound states and dressed atoms," *Phys. Rev. Lett.* **64**, pp. 2418–2421, 1990.
7. S. Fan, P. R. Villeneuve, J. D. Joannopoulos, and E. F. Schubert, "High extraction efficiency of spontaneous emission from slabs of photonic crystals," *Phys. Rev. Lett.* **78**, pp. 3294–3297, 1997.
8. O. Painter, R. K. Lee, A. Yariv, A. Scherer, J. D. O'Brien, P. D. Dapkus, and I. Kim, "Two-dimensional photonic crystal defect laser," *Science* **284**, pp. 1819–1821, 1999.
9. A. Erchak, D. J. Ripin, S. Fan, P. Rakich, J. D. Joannopoulos, E. P. Ippen, G. S. Petrich, and L. A. Kolodziejski, "Enhanced coupling to vertical radiation using a two-dimensional photonic crystal in a semiconductor light-emitting diode," *Appl. Phys. Lett.* **78**, pp. 563–565, 2001.
10. S. Noda, M. Yokoyama, M. Imada, A. Chutinan, and M. Mochizuki, "Polarization mode control of two-dimensiona; photonic crystal laser by unit cell structure design," *Science* **293**, pp. 1123–1125, 2001.
11. A. Mekis, J. C. Chen, I. Kurland, S. Fan, P. R. Villeneuve, and J. D. Joannopoulos, "High transmission through sharp bends in photonic crystal waveguides," *Phys. Rev. Lett.* **77**, pp. 3787–3790, 1996.
12. S. Fan, P. R. Villeneuve, J. D. Joannopoulos, and H. A. Haus, "Channel drop tunneling through localized states," *Phys. Rev. Lett.* **80**, pp. 960–963, 1998.
13. J. C. Knight, J. Broeng, T. A. Birks, and P. S. J. Russell, "Photonic band gap guidance in optical fibers," *Science* **282**, pp. 1476–1478, 1998.

14. R. F. Cregan, B. J. Mangan, J. C. Knight, T. A. Birks, P. S. J. Russell, P. J. Roberts, and D. C. Allan, "Single-mode photonic band gap guidance of light in air," *Science* **285**, pp. 1537–1539, 1999.
15. S. G. Johnson, S. Fan, P. R. Villeneuve, J. D. Joannopoulos, and L. A. Kolodziejski, "Guided modes in photonic crystal slabs," *Phys. Rev. B* **60**, pp. 5751–5758, 1999.
16. M. Ibanescu, Y. Fink, S. Fan, E. L. Thomas, and J. D. Joannopoulos, "An all-dielectric coaxial waveguide," *Science* **289**, pp. 415–419, 2000.
17. S.-Y. Lin, V. M. Hietala, L. Wang, and E. D. Jones, "Highly dispersive photonic band-gap prism," *Opt. Lett.* **21**, pp. 1771–1773, 1996.
18. H. Kosaka, T. Kawashima, A. Tomita, M. Notomi, T. Tamamura, T. Sato, and S. Kawakami, "Superprism phenomena in photonic crystals," *Phys. Rev. B* **58**, pp. R10096–R10099, 1998.
19. B. Gralak, S. Enoch, and G. Tayeb, "Anomalous refractive properties of photonic crystals," *J. Opt. Soc. Am. A* **17**, pp. 1012–1020, 2000.
20. M. Notomi, "Theory of light propagation in strongly modulated photonic crystals: refractionlike behavior in the vicinity of the photonic band gap," *Phys. Rev. B* **62**, pp. 10696–10705, 2000.
21. V. G. Veselago, "The electrodynamics of substances with simultaneously negative values of ϵ and μ," *Sov. Phys. Usp.* **10**, pp. 509–514, 1968.
22. D. R. Smith, W. J. Padilla, D. C. View, S. C. Nemat-Nasser, and S. Schultz, "Composite medium with simultaneously negative permeability and permittivity," *Phys. Rev. Lett.* **84**, pp. 4184–4187, 2000.
23. R. A. Shelby, D. R. Smith, and S. Schultz, "Experimental verification of a negative index of refraction," *Science* **292**, pp. 77–79, 2001.
24. J. B. Pendry, "Negative refraction makes a perfect lens," *Phys. Rev. Lett.* **85**, pp. 3966–3969, 2000.
25. T. Baba and M. Nakamura, "Photonic crystal light deflection devices using the superprism effect," *IEEE J. Quantum Electron.* **38**, pp. 909–914, 2002.
26. L. Wu, M. Mazilu, T. Karle, and T. F. Krauss, "Superprism phenomena in planar photonic crystals," *IEEE J. Quantum Electron.* **38**, pp. 915–918, 2002.
27. T. Baba and T. Matsumoto, "Resolution of photonic crystal superprism," *Appl. Phys. Lett.* **81**, pp. 2325–2327, 2002.
28. J. Bravo-Abad, T. Ochiai, and J. Sanchez-Dehesa, "Anomalous refractive properties of a two-dimensional photonic band-gap prism," *Phys. Rev. B* **67**, p. 115116, 2003.
29. T. Ochiai and J. Sanchez-Dehesa, "Superprism effect in opal-based photonic crystals," *Phys. Rev. B* **64**, p. 245113, 2001.
30. T. Prasad, V. Colvin, and D. Mittleman, "Superprism phenomenon in three-dimensional macroporous polymer photonic crystals," *Phys. Rev. B* **67**, p. 165103, 2003.
31. C. Luo, S. G. Johnson, J. D. Joannopoulos, and J. B. Pendry, "All-angle negative refraction without negative index," *Phys. Rev. B* **65**, p. 201104(R), 2002.
32. C. Luo, S. G. Johnson, and J. D. Joannopoulos, "All-angle negative refraction in a three-dimensionally periodic photonic crystal," *Appl. Phys. Lett.* **81**, pp. 2352–2354, 2002.
33. C. Luo, S. G. Johnson, J. D. Joannopoulos, and J. B. Pendry, "Negative refraction without negative index in metallic photonic crystals," *Opt. Express* **11**, pp. 746–754, 2003.
34. C. Luo, S. G. Johnson, J. D. Joannopoulos, and J. B. Pendry, "Subwavelength imaging in photonic crystals," *Phys. Rev. B* **68**, p. (in press), 2003.
35. A. Yariv and P. Yeh, *Optical Waves in Crystals: Propagation and Control of Laser Radiation*, Wiley, New York, 1984.
36. S. G. Johnson and J. D. Joannopoulos, "Block-iterative frequency-domain methods for maxwell's equations in a planewave basis," *Opt. Express* **8**, pp. 173–190, 2001.
37. D. M. Whittaker and I. S. Culshaw, "Scattering-matrix treatment of patterned multilayer photonic structures," *Phys. Rev. B* **60**, pp. 2610–2618, 1999.
38. T. Baba and D. Ohsaki, "Interfaces of photonic crystals for high efficiency light transmission," *Jpn. J. Appl. Phys.* **40**, pp. 5920–5924, 2001.
39. S. G. Johnson, P. Bienstman, M. A. Skorobogatiy, M. Ibanescu, E. Lidorikis, and J. D. Joannopoulos, "Adiabatic theorem and continuous coupled-mode theory for efficient taper transitions in photonic crystals," *Phy. Rev. E* **66**, p. 066608, 2002.